

# Variational Adaptive Gaussian Decomposition: Scalable Quadrature-Free Time-Sliced Thawed Gaussian Dynamics

Rahul Sharma and Amartya Bose<sup>a)</sup>

Department of Chemical Sciences, Tata Institute of Fundamental Research, Mumbai 400005, India

Time-slicing has emerged as a strategy for incorporating semiclassical propagation into real-time path integral formulation and recovering full quantum dynamics. A central step is the decomposition of a time-evolved wave function into a superposition of Gaussian wave packets (GWPs). Here we introduce a quadrature-free variational framework for GWP decomposition, reformulating it as an optimization problem in which the GWP parameters are chosen to maximize the overlap with the time-evolving wave function. An autoencoder-decoder neural network is used for this optimization, with the representation being adaptively reoptimized during propagation. Each wave packet in this decomposition represents a localized patch of the underlying semiclassical manifold, while retaining full correlations between all degrees of freedom. This variational adaptive Gaussian decomposition (VAGD) approach yields a compact Gaussian expansion, providing a scalable route to time-sliced semiclassical quantum dynamics. While general, applying VAGD to facilitate time-slicing of thawed Gaussian approximation (TGA) allows a route to improving the semiclassical treatment to the full quantum mechanical result in a systematic manner.

## I. INTRODUCTION

Much of chemistry can be formulated in terms of the time-evolution of systems governed by quantum mechanics. However, simulating the time-dependent Schrödinger equation poses significant computational challenges as the complexity grows exponentially with the number of degrees of freedom. Formally exact methods for wave-function propagation such as the family of multi-configurational time-dependent Hartree methods ((ML-)MCTDH)<sup>1,2</sup> are able to handle the systems with up to a few tens of degrees of freedom. However, despite their remarkable efficiency, these methods are limited by the growing Hilbert space dimensionality. Consequently, approximate approaches that exploit classical insights prove to be very powerful. Owing to Bohr’s Correspondence Principle and the relatively large masses of atoms and molecules, these semiclassical schemes of propagation have, over the years, emerged as a framework of accurate approximations to the full quantum dynamics.<sup>3</sup> These methods also have the added advantage that they can be applied to arbitrary potential energy landscapes in an approximate manner.

Among the many semiclassical techniques that have been developed, two prominent classes are those based on stationary-phase approximation of the path integral<sup>4-6</sup> and the thawed Gaussian approximation<sup>7-11</sup> (TGA). TGA is a particularly attractive approximate technique that describes the motion of a Gaussian wave packet (GWP) whose width and orientation can evolve dynamically on an arbitrary potential energy surface. Simpler versions of this method have even been applied to study molecular systems in an *ab initio* manner.<sup>12-16</sup> While

extremely attractive, the accuracy of these semiclassical methods typically deteriorates at long propagation times. A crucial approach to improving this is the idea of re-expanding the time-dependent wave-function into a superposition of Gaussian wave packets (GWPs) or time-slicing.<sup>17-19</sup> This Gaussian decomposition is done at intervals beyond which the semiclassical propagation falters. Similar ideas are at the heart of Gaussian MCTDH,<sup>20</sup> its system-bath versions,<sup>21-23</sup> and the related multi-level methods.<sup>24</sup>

In improving semiclassical propagation at long times, there are two challenges, therefore, that must be addressed: (1) the efficiency of the algorithm for time-slicing for a multidimensional system; (2) the number of resultant Gaussians in the decomposed wave function. The first is a challenge because the procedure for decomposing a wave function into many Gaussians involves multidimensional integrals. Although Monte Carlo-based methods are often the most practical methods for handling such multidimensional integrals, they become inefficient when the integrand has both positive and negative parts. In such cases, phase cancellation leads to an exponential growth of variance, giving rise to the infamous Monte Carlo “sign problem”, which becomes increasingly severe with dimensionality. Moreover, even wave functions that are initially real acquire complex phases during time-evolution leading to the “dynamical sign-problem.”

Kong, Markmann, and Batista<sup>19</sup> showed that using a Husimi transform expansion one can solve even the strongly correlated problem of dynamics in a two-dimensional double well potential at full quantum levels of accuracy using the time-sliced TGA (TSTG). While TSTG avoids the Monte Carlo sign problem through an innovative use of fast Gaussian transforms, it is still inherently quadrature-based. Consequently, the number of Gaussians, and therefore classical trajectories, grows exponentially with the system dimensionality. This scaling severely limits the practical applicability of TSTG in

<sup>a)</sup>Electronic mail: [amartya.bose@tifr.res.in](mailto:amartya.bose@tifr.res.in); Electronic mail: [amartya.bose@gmail.com](mailto:amartya.bose@gmail.com)

combination with *ab initio* molecular dynamics.

In this work, we propose an alternative approach to Gaussian wave function decomposition that circumvents both the problems. The key insight is to reformulate time-slicing as an optimization problem in which the parameters of the GWPs constituting the decomposed output are determined variationally, using an autoencoder-decoder neural network, to maximize the overlap with the input wave function. This variational adaptive Gaussian decomposition (VAGD) method is quadrature-free, which allows for multidimensional applications, and produces an optimally compact representation, minimizing the number of classical trajectories generated. VAGD is general, and can be used in conjunction with any semiclassical propagation to enable time-slicing.

This paper is organized as follows. Time-sliced TGA is introduced in Sec. II A to provide a context. VAGD is introduced in Sec. II B, with numerical demonstrations in Sec. III. We illustrate dimensional scaling and tunneling systems as examples. Finally, we end with some concluding remarks in Sec. IV.

## II. METHODS

### A. Time-Sliced Thawed Gaussian

The time-evolution of an initial wave-function  $|\psi_0\rangle$  of a  $d$ -dimensional system, under a Hamiltonian,  $\hat{H} = \frac{1}{2} \sum_j \frac{\hat{P}_j^2}{M_j} + V(\{\hat{X}_j\})$  is given by

$$|\psi(t)\rangle = \exp\left(-\frac{i}{\hbar} \hat{H}t\right) |\psi_0\rangle. \quad (1)$$

Depending upon the particular semiclassical approximation used, the propagator,  $\exp(-i\hat{H}t/\hbar)$ , is represented in different ways using classical trajectories. Under the thawed Gaussian wave-packet (GWP) propagation,<sup>7</sup> the time-dependent wave function is presumed to be approximated as a GWP:

$$\langle \vec{x} | \psi(t) \rangle = \exp\left(\frac{i}{2} (\vec{x} - \vec{q}_t)^T A_t (\vec{x} - \vec{q}_t) + \frac{i}{\hbar} \vec{p}_t^T (\vec{x} - \vec{q}_t) + i\gamma_t\right) \quad (2)$$

where under the local harmonic approximation, the ‘‘position’’ and ‘‘momenta’’ coordinates,  $\vec{q}_t$  and  $\vec{p}_t$  respectively, satisfy the classical equations of motion,

$$\dot{\vec{q}}_t = M^{-1} \vec{p}_t \quad (3)$$

$$\dot{\vec{p}}_t = -\vec{\nabla}V(\{\vec{q}_t\}) \quad (4)$$

where  $M$  is the diagonal mass matrix. The ‘‘width’’ matrix,  $A_t$ , and the generalized phase,  $\gamma_t$  satisfy the follow-

ing equations:

$$\dot{A}_t = -2A_t M^{-1} A_t - \frac{1}{2} \nabla^2 V(\{\vec{q}_t\}) \quad (5)$$

$$\dot{\gamma}_t = i\hbar \text{Tr}(M^{-1} A_t) + \sum_j \frac{p_j^2}{2M_j} - V(\{\vec{q}_t\}). \quad (6)$$

While exact for harmonic potentials, owing to the impact of the non-zero higher-order derivatives of the anharmonic potentials, the quality of TGA deteriorates with time even when the initial state is a Gaussian. As outlined originally in Ref. 17, this deterioration can be alleviated by essentially using the semiclassical propagator as an ingredient for a path integral simulation. The essential idea is to propagate with TGA till the prescription starts to break down, at which point, the wave function is re-expressed as a superposition of localized GWPs. Each of these wavepackets are then individually propagated once again till the next decomposition step. The number of time-steps between consecutive decomposition steps is a convergence parameter, and denoted by  $N_{\text{seg}}$ .

One possible implementation of this re-expansion can be in terms of the over-complete coherent state basis. However, an immediate challenge that ensues is that the resultant multidimensional integrals are not amenable to Monte Carlo simulations owing to the accumulation of pure phase with time-propagation. A Husimi transformed expansion-based implementation of this time-sliced TGA has recently been demonstrated.<sup>19</sup> Despite its success, the Husimi-based TSTG remains quadrature-dependent and scales poorly with system dimensionality, motivating the need for a quadrature-free, variational approach to GWP decomposition.

### B. Variational Adaptive Gaussian Decomposition (VAGD)

We introduce a variational approach for constructing an optimized Gaussian representation of an arbitrary input wave function. In the context of VAGD with TGA, the normalized input wave function is written as a sum of  $N_{\text{inp}}$  Gaussians,  $|\psi\rangle = \sum_{j=1}^{N_{\text{inp}}} c_j |\phi_j\rangle$ . The goal is to find a new representation in terms of  $N_{\text{out}}$  Gaussians,  $|\Psi\rangle = \sum_{j=1}^{N_{\text{out}}} C_j |\Phi_j\rangle$ . Here,  $N_{\text{out}}$  is capped at a certain user-defined maximum number,  $K$ . An exact decomposition requires that the magnitude of the overlap of the input and output wave functions, called the fidelity, is unity,  $F_{\text{exact}} = |\langle \psi | \Psi \rangle| = 1$ . We, therefore, develop a variational approach to maximizing this fidelity to a threshold value,  $F_{\text{thresh}}$ . The exact  $N_{\text{out}}$  that is used is adjusted adaptively, with the *optimal* representation being defined as the one that achieves the target fidelity using a minimum  $N_{\text{out}}$ .

The optimized representation is obtained through a variational procedure that minimizes a loss defined in terms of the fidelity,

$$\mathcal{L} = -\log(F) + (1 - F), \quad (7)$$

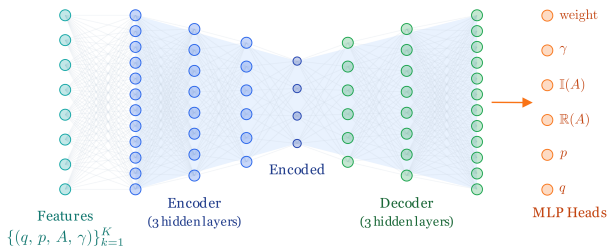


FIG. 1: Schematic of auto-encoder decoder setup which acts as the basis transformation.

which is equivalent to maximizing the fidelity between an input wave function and its Gaussian expansion. The optimization is implemented using an autoencoder-decoder neural network. Figure 1 shows a schematic of the architecture, which maps the input wave function to the set of parameters defining the output representation via a low-dimensional “encoded” layer. The network is optimized such that the loss, which depends upon the input and the output representations, is minimized, ensuring that the resulting parameters encode a faithful Gaussian decomposition of the input wave function.

It is important to emphasize that, unlike typical uses of autoencoder-decoder architectures in which the low-dimensional latent “encoded” space representation is of interest, here the focus is on the optimized output of the decoder. This output,  $|\Psi\rangle$ , encodes a different but faithful representation of the input wave function,  $|\psi\rangle$ . In this framework, the neural network serves merely as a numerical optimizer for obtaining the parameters for the Gaussian decomposition.

With this perspective, it is not necessary to train a generically applicable neural network. Instead, the network is optimized specifically for each wave function under consideration. In applications where the propagation of classical trajectories is the computational bottleneck, the additional cost associated with the optimization is negligible. In fact, it is even beneficial to increase the time for a proper optimization in an attempt to decrease the number of classical trajectories. Moreover, because the network is used as a variational optimizer rather than a predictive model, the usual challenges associated with neural networks, such as the construction of representative training sets and concerns about overfitting, are not relevant here. In a sense, the variational optimization adaptively identifies the set of Gaussian wave packets that best cover the relevant region of phase space explored by the input wave function.

Finally, we discuss how  $N_{\text{out}}$  is determined. The optimal representation is defined by the minimum number of Gaussians used, or minimum  $N_{\text{out}}$ , required to achieve  $F_{\text{thresh}}$ , essential for reducing the number of classical tra-

jectories. However, as end-users, we only set  $K$ , which is an upper limit to  $N_{\text{out}}$ . The algorithm starts with an initial guess of  $N_{\text{out}} = N_{\text{inp}}$ . If upon optimization, the threshold fidelity,  $F_{\text{thresh}}$ , is not achieved, then the value of  $N_{\text{out}}$  is increased by a user-specified step size  $\Delta N$  and the network is reoptimized. The process is repeated till either the threshold fidelity is successfully achieved or the upper limit of  $K$  is reached. We refer to this procedure as an adaptive basis expansion technique, which ensures an optimal Gaussian decomposition.

## 1. Encoding of Parameters

To construct the input to the neural network and reconstruct the wave function from the neural network, it is necessary to specify the parameters. A generic  $d$ -dimensional GWP, Eq. (2), is parameterized by two  $d$ -dimensional real “phase space” vectors,  $(\vec{q}, \vec{p})$ , the  $d \times d$  complex  $A$  matrix, and the single complex number,  $\gamma$ , representing the phase. Considering that the  $A$  matrix has to be symmetric,  $\frac{d(d+1)}{2}$  complex numbers, can uniquely encode it. Therefore,  $d^2 + 3d + 2$  real numbers can be used to represent a single GWP. So the input to the autoencoder-decoder has  $N_{\text{inp}} \times (d^2 + 3d + 2)$  input parameters.

Now the interpretation of the output is largely similar, with the  $(\vec{q}, \vec{p})$  and  $\gamma$ , retained. The main difference comes in the  $A$  matrix: the real part of  $A$ ,  $A^{\text{R}}$ , must be symmetric, but the imaginary part of  $A$ ,  $A^{\text{I}}$ , which encodes the wave packet width, must additionally be positive definite. Directly optimizing  $A^{\text{I}}$  during training does not guarantee this property. To ensure positive definiteness by construction, we optimize a lower triangular matrix,  $L$ , with positive diagonal elements for each GWP. The width matrix of the  $k$ th Gaussian is finally reconstructed using a Cholesky decomposition,  $A_k^{\text{I}} = L_k L_k^T$ .

This completes the discussion on the basic version of the VAGD algorithm. There are some numerical considerations that help with optimizing the network faster. We discuss these subtleties in the next section.

## 2. Numerical Stabilization Strategies

VAGD, as defined so far, allows for arbitrarily broad Gaussians to be incorporated in the decomposition if required. While broad Gaussians may help minimize the number of trajectories, the local harmonic approximation is violated sooner for them than for the narrow wave packets, necessitating a more frequent decomposition to maintain accuracy. This issue can be mitigated by putting a dimension-specific, user-defined cap on the width of each Gaussian, which effectively sets a lower limit on the diagonal values of imaginary parts of  $A_k$ , such that  $(A_k^{\text{I}})_{j,j} \geq (W_{\text{min}})_j$  for all dimension,  $j$ .

A direct implementation of a VAGD decomposition step as described till now starts from a randomly ini-

tialized network, which increases the number of optimization cycles, or epochs, required for convergence to  $F_{\text{thresh}}$ . Additionally, the position and the width of the wave function can fluctuate significantly during time-evolution, which makes the numerical optimization of the neural network difficult. We will see that these two difficulties are closely related.

A natural way to address the randomly initialized starting network problem is to use a “warm-start” ansatz. The fundamental intuition is that between consecutive decomposition steps, the wave function may not have significantly changed in shape. Instead of starting from a random network, one can therefore reuse the optimized network from the previous step, potentially reducing the number of epochs of training required.

However, while the intuition holds for the shape of the wave function, its position can still change quite substantially between decomposition steps. As a result, a direct warm-start ansatz may still lead to unstable or ineffective optimizations. To stabilize the numerics and also maximize the effectiveness of the warm-start ansatz, the wave functions are “regularized” to some common scale.

This regularization consists of two preprocessing steps. First, the wave function is recentered to remove its average position. Second, the coordinate axes are rescaled so that the wave function has variances comparable to the initial state. The neural network is trained on this pre-processed wave function. After optimization, the regularization transformation is undone to recover the physical representation.

### III. NUMERICAL ILLUSTRATIONS

We demonstrate the utility of VAGD by using it in conjunction with time-sliced TGA to converge to the true quantum mechanical results. VAGD in this context is used to generate an optimal representation of the time-evolved wave function at every decomposition step. We shall refer to this combination as VAGD-TGA. The split-operator Fourier transform (SOFT)<sup>25,26</sup> method is used to generate the numerically exact dynamics that will be the point of comparison.

#### A. Morse Potential

We start our exploration with the dynamics of wave packets in Morse potentials. In Sec. III A 1, we explore the convergence of VAGD-TGA to the full quantum results under different levels of anharmonicity. Subsequently in Sec. III A 2, we study the scaling of the algorithm by looking at the dynamics under multidimensional independent Morse oscillators.

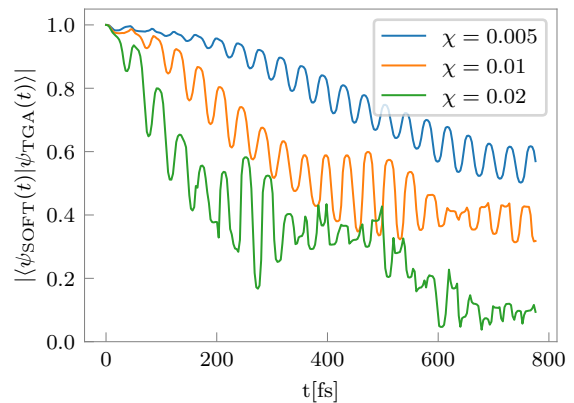


FIG. 2: Breakdown of TGA with anharmonicity of 1D Morse potential.

#### 1. 1D Explorations

First consider a 1D Morse oscillator:

$$V(x) = D_e [1 - \exp(-a(x - x_{\text{eq}}))]^2, \quad (8)$$

where  $D_e$  is the dissociation energy,  $a$  is the width of the well, and  $x_{\text{eq}}$  is the equilibrium bond distance. It is often more convenient to think in terms of the harmonic frequency at the bottom of the well,  $\omega = a\sqrt{2D_e}$ , and an anharmonicity factor,  $\chi = \frac{\omega}{4D_e}$ ,<sup>14</sup> which is zero for harmonic potentials. The parameters,  $D_e$  and  $a$  can be simply obtained by inverting the relations.

In Fig. 2, we show the overlap of the wave function evolved using the traditional TGA with the numerically exact SOFT simulations for different values of  $\chi$ . Following the examples in Ref. 14, the equilibrium bond length  $x_{\text{eq}} = 20.95 a_0$  and  $\omega = 900 \text{ cm}^{-1}$ . The initial wave packet is taken to be a real Gaussian centered at  $q_0 = 0$ , with  $A = -\frac{\omega_0}{\hbar}$ , where  $\omega_0 = 1000 \text{ cm}^{-1}$ . The simulations were run with a time-step of  $\Delta t = 0.053 \text{ fs}$ . Consistent with our expectations, the quality of TGA deteriorates with time, and this deterioration is faster for larger values of  $\chi$ .

Now, we explore our VAGD method. We perform the variational decomposition with  $N_{\text{seg}} = 50$ . At each decomposition boundary, the reconstructed state is required to satisfy  $F_{\text{thresh}} = 0.9995$  with the propagated wavefunction. The width parameter,  $W_{\text{min}}$ , was set to 5.

Consider the case of  $\chi = 0.005$  as a first example. In Fig. 3, we examine the improvement of VAGD with increasing  $K$ . There is a clear and systematic improvement of the overlap with the SOFT result with the maximum number of GWPs allowed,  $K$ . This improvement is most clearly observed at longer times, as the quality of the semiclassical approximation gets worse. By  $K \geq 6$ , the VAGD-TGA becomes practically identical to SOFT. For this example, we push the limits and claim convergence at  $K = 8$ .

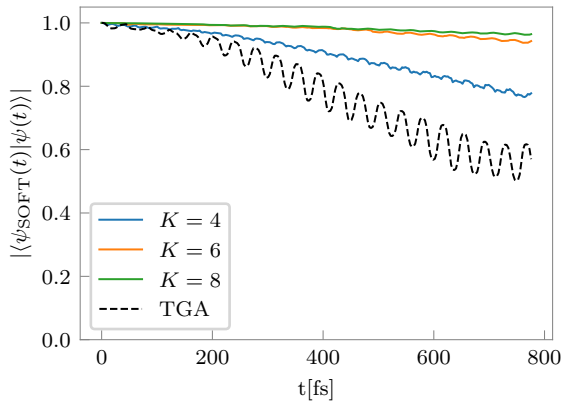


FIG. 3: Overlap of the VAGD-TGA method with the SOFT wave function for different maximum number of Gaussians.

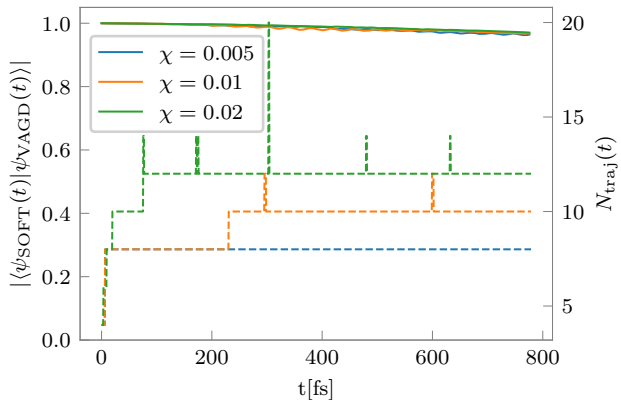


FIG. 4: Overlap of VAGD-TGA wave function with SOFT solution (solid, left  $y$ -axis) and number of VAGD trajectories (dashed, right  $y$ -axis) of 1D-Morse oscillator for different values of  $\chi$ .

On increasing anharmonicity, while  $\chi = 0.01$  converged with the same  $N_{\text{seg}}$ ,  $\chi = 0.02$  required more frequent decompositions with  $N_{\text{seg}} = 25$ . We show the overlap and the number of trajectories for the converged simulation in Fig. 4. The convergence gets more difficult with anharmonicity. One way to think about this is greater the anharmonicity, quicker is the breakdown of the local harmonic approximation for GWPs of the same width. Therefore, we need to perform the VAGD steps more frequently.

The number of trajectories,  $N_{\text{traj}}(t)$ , also shown in Fig. 4, grows with time demonstrating the build-up of the effects of anharmonicity and deviation from the basic thawed Gaussian ansatz. However, what is extremely heartening is that the number of trajectories required is relatively small in all the cases. This becomes especially important when running *ab initio* dynamics where trading the cost of a better decomposition for fewer number

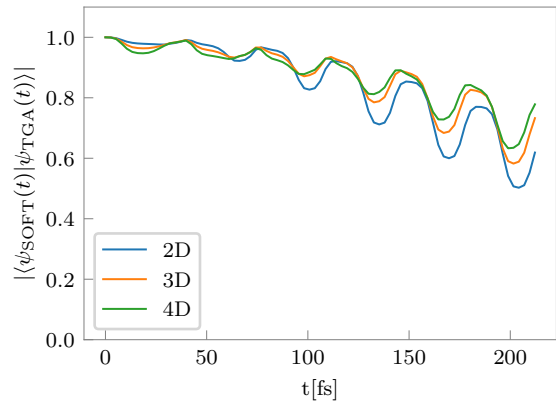


FIG. 5: Overlap of TGA solutions with the SOFT solution for multidimensional Morse models as a function of dimensionality.

of trajectories can prove to be extremely lucrative. Moreover, depending on the physics of the problem at hand, the actual number of trajectories may be substantially less than the upper limit  $K$  provided. This is another benefit of the adaptive algorithm. We emphasize that checking the overlap with the numerically exact SOFT results is by far the most stringent test of the correctness of the method. Other observables, like correlation functions, that are crucial for spectra, would converge with far fewer trajectories.

## 2. Multidimensional Explorations

Pushing the semiclassical simulations to the full quantum levels of accuracy gets increasingly difficult with dimensionality. The time-slicing procedure, if done using quadrature, can very quickly become intractable. To study the scaling of VAGD with dimensions, consider the simple case of  $d$  uncoupled Morse oscillators as an example:

$$V(\vec{x}) = D \sum_{i=1}^d (1 - \exp[-a(x_i - x_{0,i})])^2, \quad (9)$$

where all the centers at origin ( $x_{0,i} = 0.0$ ) and  $\omega = 900 \text{ cm}^{-1}$  and  $\chi = 0.005$  for all dimensions. While the scaling with dimensionality would of course be worse for cases where the different dimensions are correlated, this independent dimensional model allows us to study the scaling in a relatively simplified setting. Our time-sliced TGA does not “know” that the dimensions can be separated and hence does not use that information explicitly. We will explore correlated multidimensional models in terms of the double-well potentials.

For the multidimensional Morse calculations, the ini-

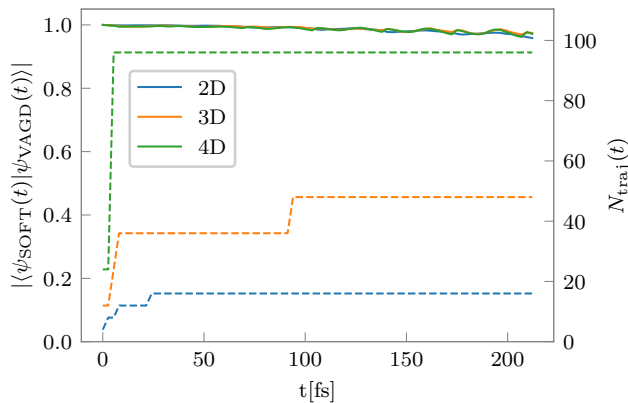


FIG. 6: Overlap of VAGD-TGA wave function with SOFT solution (solid, left  $y$ -axis) and number of trajectories (dashed, right  $y$ -axis) for multidimensional Morse models as a function of dimensionality.

tial wavefunction is taken as

$$\Psi(\mathbf{x}, 0) = N \exp \left[ -\frac{\omega}{2\hbar} \sum_{i=1}^d \left( x_i + \sqrt{\frac{8}{d}} \right)^2 \right], \quad (10)$$

with zero initial momentum. We start by demonstrating the deterioration of the quality of the standard TGA simulation for different dimensionality of the system in Fig. 5. A time-step of  $\Delta t = 0.053$  fs was used for all the calculations. Because the dimensions are independent and the displacement of the initial wave packet along each dimension decreases with  $d$ , the degradation of quality of TGA is less pronounced for larger  $d$ .

Next, we perform the VAGD procedure every 25 steps. At each decomposition boundary, the VAGD-reconstructed state is required to satisfy  $F_{\text{thresh}} = 0.9995$  with the propagated and the  $W_{\text{min}}$  for individual Gaussian wave packets was set to 5.0 along each dimension. The results shown in Fig. 6 demonstrate the recovery of full quantum mechanical results. In all these cases, the number of trajectories saturated to the maximum limit allowed,  $K$ . However, there are a couple of things to be noted. First, the number of trajectories do not immediately converge to  $K$ . Depending upon the exact system setup, it can use less trajectories as well. This is the adaptive nature of the algorithm. The threshold  $K$  that is required is also a function of the duration of simulation. The longer a wave packet propagates in an anharmonic potential, the more non-Gaussian character it develops, and the higher is the number of trajectories that are required.

Finally, in Fig. 7, we summarize the number of trajectories required to obtain the converged results at a final time of  $t_{\text{final}} = 212$  fs. It is important, however, to interpret Fig. 7 only as an empirical summary of the present numerical experiments. Therefore, we do not make any broader claim regarding a universal scaling law

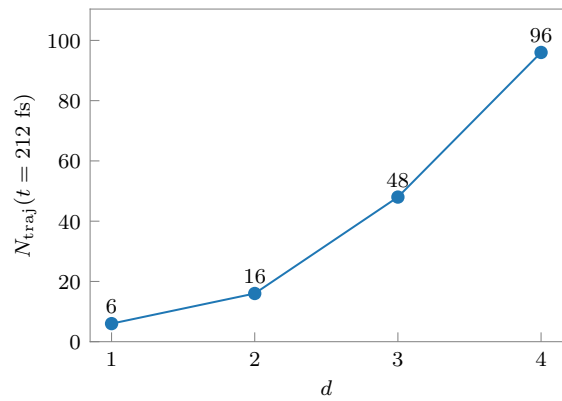


FIG. 7: Number of trajectories required for converged results at  $t = 212$  fs for different numbers of dimensions.

from these data alone. Nevertheless, the trend provides a useful indication of how the complexity of the adaptive Gaussian representation grows for these multidimensional Morse calculations.

## B. Double Well Potentials

As a next class of more complicated examples, we demonstrate VAGD method on the double-well potential. These systems are dynamically strongly correlated in time, in the sense that no single classical trajectory can capture the true dynamics. The deep tunneling observed in these systems cannot be described by simple single trajectory methods, and therefore, TGA fails. Time-sliced TGA has been shown to be able to account for the tunneling event.<sup>19</sup> We demonstrate how VAGD is able to optimally represent the wave-function in one- and two-dimensions.

### 1. One-Dimensional Problem

Following Ref. 19, the 1D double well potential is defined to be:

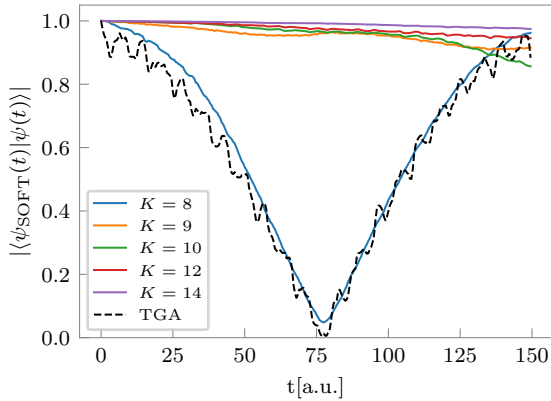
$$V_{\eta}(x) = \frac{x^4}{16\eta} - \frac{x^2}{2}, \quad \eta > 0. \quad (11)$$

There are two minima at  $x_{\pm} = \pm 2\sqrt{\eta}$  separated by a barrier at  $x = 0$ . Consistent with Ref. 19, we use  $\eta = 1.3544$ , so that the minima are located at  $x_{\pm} \approx \pm 2.329$ . We use an initial GWP localized in the left well,

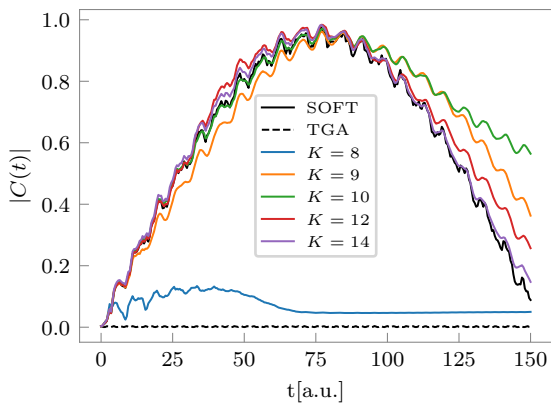
$$\Psi(x, 0) = \pi^{-1/4} \exp \left( -\frac{1}{2} (x + 2\sqrt{\eta})^2 \right), \quad (12)$$

with zero momentum.

The simulations were done using a time step of  $\Delta t = 0.01a$  u and VAGD was performed every 20 steps ( $N_{\text{seg}} =$



(a) Overlap of TGA and VAGD-TGA wave functions with SOFT as a function of time



(b) Comparison of  $|C(t)|$  at different levels of approximation.

FIG. 8: Accuracy of the VAGD-TGA scheme for the 1D double well.

20) with a  $F_{\text{thresh}} = 0.9999$ . In contrast to the Morse tests above, this relatively more frequent decomposition is necessary for the double well because the local harmonic approximation deteriorates more rapidly in this strongly anharmonic landscape and the basis must be refreshed more often to maintain accuracy.

In addition to the overlap with SOFT results, following Ref. 19, we correlate the mirror-image of the initial wave function with the time-propagated one,

$$C(t) = \int dx \Psi^*(-x, 0)\Psi(x, t), \quad (13)$$

measuring the extent of tunneling captured by the various levels of approximation.

In Fig. 8, we show the overlap of the semiclassical solutions with the SOFT wave function (Fig. 8 (a)) and the absolute value of the mirror correlation function, Eq. 13 (Fig. 8 (b)). The VAGD procedure used  $W_{\text{min}} = 5.0$ . From the overlaps, we see that the TGA result falters immediately, giving an overlap of almost 0.0 at  $t \approx 75 a.u.$ ,

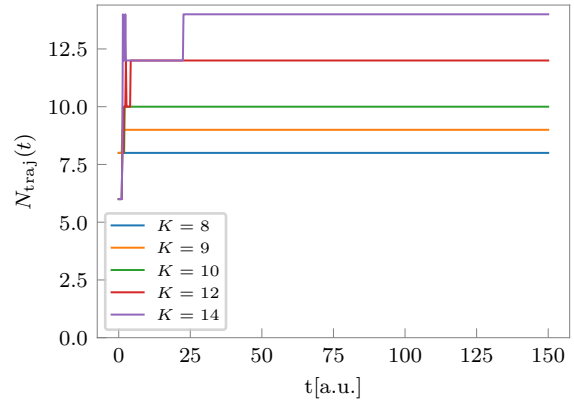


FIG. 9: Number of trajectories for the 1D double well system.

at which time the wavefunction has completely tunneled from the left to the right well. This first tunneling event corresponds to the maximum of  $|C(t)|$  at around  $t \approx 75 a.u.$  The subsequent lowering of the correlation function corresponds to the wave function tunneling back to the initial well.

Notice in Fig. 8 (b), the TGA wave function does not tunnel at all. This is expected because of its purely classical nature. It is interesting that in our VAGD-TGA simulations, upto  $K = 8$ , the wave function does not really tunnel. As we move from  $K = 8$  to  $K = 9$ , there is a jump in the amount of tunneling captured. Qualitatively, all the essential features of  $|C(t)|$  is achieved by a  $K = 9$  calculation, though the quantitative agreement is still missing. It is the second tunneling event back to the original well that proves to be even more challenging. Using a maximum of  $K = 14$  trajectories, we start to get quantitative agreement of the correlation function upto a maximum time of  $t = 150$ . This is a significant improvement over the original TSTG method,<sup>19</sup> which used 2048 trajectories in comparison to VAGD method using tens of trajectories.

In Fig. 9, we show the actual number of trajectories used as a function of time for different values of  $K$ . We see a difference from the previous examples. Here, the number of trajectories almost immediately jumps to the maximum value owing to the significantly greater degree of anharmonicity. Even the adaptive algorithm is unable to effectively restrict the  $N_{\text{traj}}(t)$  to extremely low values. If we had not capped it, the number would have been even larger. However, the perfect overlaps tell us that the simulations are converged with respect to  $K$ . Using larger values of  $K$  would have resulted in the adaptive algorithm making the  $N_{\text{traj}}(t)$  significantly higher than what is required.

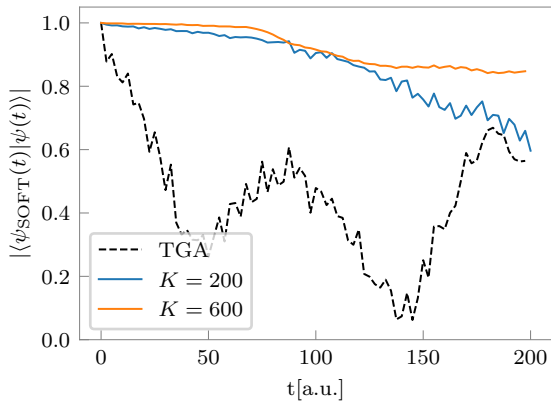


FIG. 10: Overlap of VAGD-TGA and TGA method for 2D double well potential with SOFT.

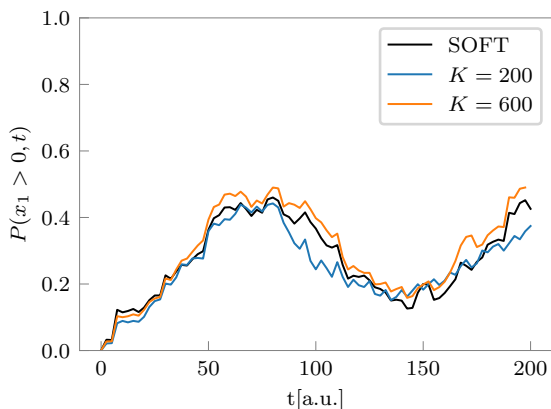


FIG. 11: Tunneling population vs time for double well.

## 2. Tunneling in a Two-Dimensional Double-Well

Finally, we explore the 2D double well studied by Kong *et al.*<sup>19</sup> The model potential couples two strongly correlated degrees of freedom and is given by

$$V_\eta(x_1, x_2) = \frac{x_1^4}{16\eta} - \frac{x_1^2}{2} + \frac{x_2^2}{2} + \frac{x_1 x_2}{2}, \quad \eta > 0. \quad (14)$$

As in the one-dimensional case, the quartic term generates a double-well structure along  $x_1$ , while the bilinear coupling term ( $x_1 x_2 / 2$ ) induces a strong correlation between the coordinates. The initial state is chosen as a single normalized GWP localized in the left well along  $x_1$ ,

$$\Psi(\vec{x}, 0) = \pi^{-1/2} \exp\left(-\frac{1}{2}((x_1 + 2\sqrt{\eta})^2 + x_2^2)\right). \quad (15)$$

Two VAGD-TGA simulations were run with  $\Delta t = 0.01 \text{ a.u.}$ , and Fig. 10 compares their results with TGA. For the present set of parameters, the  $K = 200$  calculation was carried out with  $W_{\min} = 10$  along both dimensions and  $N_{\text{seg}} = 20$ , while the improved  $K = 600$

calculation used  $W_{\min} = 25$  and  $N_{\text{seg}} = 15$ . Both the calculations were run at  $F_{\text{thresh}} = 0.99995$ . While VAGD-TGA simulations are more accurate than TGA, the overall agreement with the SOFT results remains imperfect owing to the high degree of anharmonicity. The  $W_{\min}$  of 25 enforces narrower, more localized Gaussians, so that the local harmonic approximation remains more reliable over each segment. In practice, this was paired with a smaller  $N_{\text{seg}}$  helping prevent the buildup of non-Gaussian distortions between decomposition steps.

As expected, TGA fails rapidly for this strongly correlated tunneling problem. Its overlap with the exact SOFT result drops quickly at early times and then exhibits large oscillations, indicating that a single thawed Gaussian is unable to represent the evolving correlated structure of the wave function. In contrast, both VAGD-TGA calculations retain substantially higher overlap throughout the propagation window. The  $K = 200$  result already provides a major improvement over TGA, while the  $K = 600$  calculation gives a further systematic gain and maintains better agreement at longer times and is exact up to  $t = 60 \text{ a.u.}$  For the present setup, the benefit of allowing a larger Gaussian representation becomes especially clear beyond about  $t \approx 80 \text{ a.u.}$ , where the dynamics develops stronger tunneling and interference character.

As in the previous examples, it is important to emphasize that wave-function overlap is an extremely stringent metric. It requires the approximate state to reproduce not only the spatial distribution but also the detailed phase structure of the exact quantum wave function. Therefore, even a moderate reduction in the overlap does not necessarily imply a comparable loss in the accuracy of physically relevant observables.

To examine this more directly, in Fig. 11 we show the population that has tunneled to the right half-plane,

$$P(x_1 > 0, t) = \int_0^\infty dx_1 \int_{-\infty}^\infty dx_2 |\Psi(x_1, x_2, t)|^2. \quad (16)$$

For this observable, the VAGD-TGA results track the SOFT calculation rather well throughout the entire simulation. The rise of the population during the first tunneling event, its subsequent decrease as the wave packet returns, and the re-emergence of the population at later times are all captured correctly. The  $K = 600$  calculation follows the exact result more closely. Thus, although the wave-function overlap remains the more stringent benchmark, the population observable shows that both the VAGD simulations qualitatively capture the physically relevant tunneling dynamics rather well.

## IV. CONCLUSION

The time-slicing approach<sup>17–19</sup> enables semiclassical simulations to achieve full quantum accuracy at the cost of propagating additional classical trajectories. The primary challenge, however, lies in decomposing the mul-

tidimensional time-evolved wave function into a basis of Gaussian wave packets. Monte Carlo-based approaches might appear to offer a natural solution to this problem, but in practice they are fundamentally limited by the dynamical sign problem. Even when Monte Carlo sampling can be converged, the number of trajectories required becomes prohibitively large, with the statistical error scaling as  $N^{-1/2}$  for  $N$  samples in the absence of a sign problem. Through our Variational Adaptive Gaussian Decomposition (VAGD) scheme, we demonstrate that the essential physics encoded in the wave function can instead be captured using a relatively small number of carefully selected trajectories, providing a scalable and quadrature-free route to time-sliced thawed Gaussian dynamics.

VAGD provides a variationally optimal decomposition of a given wave function in terms of GWPs. Its main advantage is that the effective “basis” is optimized specifically for the wave function under consideration through an autoencoder–decoder architecture. In combination with time-sliced TGA (VAGD–TGA), the method has been tested on the Morse potential and on one- and two-dimensional tunneling problems. Dimensional scaling was further examined using independent Morse oscillators up to four dimensions, where the computational cost was found to grow only mildly with dimensionality. Our results suggest a polynomial scaling behavior, although the precise performance can not yet be commented on from the numerical explorations. Nevertheless, VAGD promises a substantial improvement over the exponential scaling typically encountered in conventional approaches.

Particularly encouraging is the performance observed in tunneling problems. In the one-dimensional case, the tunneling dynamics becomes visible with as few as 10 trajectories, while quantum accuracy is achieved with only 14 trajectories — representing an improvement of roughly two orders of magnitude compared with the  $\sim 10^3$  trajectories required by TSTG. In two-dimensional tunneling, similarly accurate results are obtained with approximately 500–600 trajectories, whereas TSTG required millions. VAGD–TGA is extremely effective in these tunneling scenarios, where the wave function acquires interference-driven non-trivial spatial structure which cannot be captured by a single Gaussian. The adaptive multi-Gaussian representation that VAGD provides thus yields an optimally adequate representation of the complexity.

Beyond its practical efficiency, VAGD additionally offers an appealing conceptual perspective on semiclassical dynamics. The number of Gaussian wave packets required in the decomposition naturally reflects the degree of non-classical structure present in the evolving wave function. Systems exhibiting largely classical behavior can be represented with only a small number of trajectories, whereas strongly quantum phenomena, such as interference and tunneling, require richer Gaussian representations. In this sense, the adaptive Gaussian ba-

sis produced by VAGD provides a direct measure of the intrinsic quantum complexity of the dynamics. Looking forward, the approach opens the door to scalable semiclassical simulations in higher-dimensional systems and even *ab initio* molecular models, where the combination of time-sliced dynamics with adaptive Gaussian decompositions may provide an efficient route to near-quantum-accurate simulations.

- <sup>1</sup>H.-D. Meyer, U. Manthe, and L. Cederbaum, “The multi-configurational time-dependent Hartree approach,” *Chemical Physics Letters* **165**, 73–78 (1990).
- <sup>2</sup>U. Manthe and T. Weihe, “On the multi-layer multi-configurational time-dependent Hartree approach for bosons and fermions,” *The Journal of Chemical Physics* **146**, 064117 (2017).
- <sup>3</sup>W. H. Miller, “Semiclassical Methods in Chemical Physics,” *Science* **233**, 171–177 (1986).
- <sup>4</sup>J. H. Van Vleck, “The Correspondence Principle in the Statistical Interpretation of Quantum Mechanics,” *Proceedings of the National Academy of Sciences* **14**, 178–188 (1928).
- <sup>5</sup>M. F. Herman and E. Kluk, “A semiclassical justification for the use of non-spreading wavepackets in dynamics calculations,” *Chemical Physics* **91**, 27–34 (1984).
- <sup>6</sup>W. H. Miller, “An alternate derivation of the Herman–Kluk (coherent state) semiclassical initial value representation of the time evolution operator,” *Molecular Physics* **100**, 397–400 (2002).
- <sup>7</sup>E. J. Heller, “Time-dependent approach to semiclassical dynamics,” *The Journal of Chemical Physics* **62**, 1544–1555 (1975).
- <sup>8</sup>E. J. Heller, “Time dependent variational approach to semiclassical dynamics,” *The Journal of Chemical Physics* **64**, 63–73 (1976).
- <sup>9</sup>E. J. Heller, “The semiclassical way to molecular spectroscopy,” *Accounts of Chemical Research* **14**, 368–375 (1981).
- <sup>10</sup>E. J. Heller, “Cellular dynamics: A new semiclassical approach to time-dependent quantum mechanics,” *The Journal of Chemical Physics* **94**, 2723–2729 (1991).
- <sup>11</sup>J. Vaníček, “Family of Gaussian wavepacket dynamics methods from the perspective of a nonlinear Schrödinger equation,” *The Journal of Chemical Physics* **159**, 014114 (2023).
- <sup>12</sup>T. Begušić, J. Roulet, and J. Vaníček, “On-the-fly *ab initio* semiclassical evaluation of time-resolved electronic spectra,” *The Journal of Chemical Physics* **149**, 244115 (2018).
- <sup>13</sup>T. Begušić, A. Patoz, M. Šulc, and J. Vaníček, “On-the-fly *ab initio* three thawed Gaussians approximation: A semiclassical approach to Herzberg–Teller spectra,” *Chemical Physics* **515**, 152–163 (2018).
- <sup>14</sup>T. Begušić, M. Cordova, and J. Vaníček, “Single-Hessian thawed Gaussian approximation,” *The Journal of Chemical Physics* **150**, 154117 (2019).
- <sup>15</sup>T. Begušić, E. Tapavicza, and J. Vaníček, “Applicability of the Thawed Gaussian Wavepacket Dynamics to the Calculation of Vibronic Spectra of Molecules with Double-Well Potential Energy Surfaces,” *Journal of Chemical Theory and Computation* **18**, 3065–3074 (2022).
- <sup>16</sup>T. Begušić and J. Vaníček, “Finite-Temperature, Anharmonicity, and Duschinsky Effects on the Two-Dimensional Electronic Spectra from *Ab Initio* Thermo-Field Gaussian Wavepacket Dynamics,” *The Journal of Physical Chemistry Letters* **12**, 2997–3005 (2021).
- <sup>17</sup>E. J. Heller, “Wavepacket path integral formulation of semiclassical dynamics,” *Chemical Physics Letters* **34**, 321–325 (1975).
- <sup>18</sup>J. C. Burant and V. S. Batista, “Real time path integrals using the Herman–Kluk propagator,” *The Journal of Chemical Physics* **116**, 2748–2756 (2002).
- <sup>19</sup>X. Kong, A. Markmann, and V. S. Batista, “Time-Sliced Thawed Gaussian Propagation Method for Simulations of Quantum Dynamics,” *The Journal of Physical Chemistry A* **120**, 3260–3269 (2016).
- <sup>20</sup>I. Burghardt, H.-D. Meyer, and L. S. Cederbaum, “Approaches to

- the approximate treatment of complex molecular systems by the multiconfiguration time-dependent Hartree method,” *The Journal of Chemical Physics* **111**, 2927–2939 (1999).
- <sup>21</sup>I. Burghardt, M. Nest, and G. A. Worth, “Multiconfigurational system-bath dynamics using Gaussian wave packets: Energy relaxation and decoherence induced by a finite-dimensional bath,” *The Journal of Chemical Physics* **119**, 5364–5378 (2003).
- <sup>22</sup>I. Burghardt, K. Giri, and G. A. Worth, “Multimode quantum dynamics using Gaussian wavepackets: The Gaussian-based multiconfiguration time-dependent Hartree (G-MCTDH) method applied to the absorption spectrum of pyrazine,” *The Journal of Chemical Physics* **129**, 174104 (2008).
- <sup>23</sup>S. Römer, M. Ruckebauer, and I. Burghardt, “Gaussian-based multiconfiguration time-dependent Hartree: A two-layer approach. I. Theory,” *The Journal of Chemical Physics* **138**, 064106 (2013).
- <sup>24</sup>F. D. Maiolo, G. A. Worth, and I. Burghardt, “Multi-layer Gaussian-based multi-configuration time-dependent Hartree (ML-GMCTDH) simulations of ultrafast charge separation in a donor–acceptor complex,” *The Journal of Chemical Physics* **154**, 144106 (2021).
- <sup>25</sup>M. Feit, J. Fleck, and A. Steiger, “Solution of the Schrödinger equation by a spectral method,” *Journal of Computational Physics* **47**, 412–433 (1982).
- <sup>26</sup>D. Kosloff and R. Kosloff, “A fourier method solution for the time dependent Schrödinger equation as a tool in molecular dynamics,” *Journal of Computational Physics* **52**, 35–53 (1983).